



# Effect of transition metal ion pairs doping on the dielectric properties of mullite derived by sol–gel route

NELSON KANDULNA<sup>1</sup>, DEBJYOTI RAY<sup>2,\*</sup> , SOUVIK PALUI<sup>2</sup>  
and SHARMI BHATTACHARYYA<sup>2</sup>

<sup>1</sup>Refractory and Traditional Ceramics Division, CSIR-Central Glass and Ceramic Research Institute, Kolkata 700 032, India

<sup>2</sup>Ceramic Engineering Division, Department of Chemical Technology, University of Calcutta, Kolkata 700009, India

\*Author for correspondence (drchemtech@caluniv.ac.in)

MS received 8 July 2023; accepted 22 September 2023

**Abstract.** In this study, highly crystallized pure mullite was synthesized using the sol–gel method, and transition metal oxides (TiO<sub>2</sub> and MoO<sub>3</sub>) were prepared and incorporated into the structure of mullite by an intensive solid-state mixing process. The derived precursor powders were compacted into tablets by hydraulic pressing and sintered at 1550°C. X-ray diffraction analysis of the sintered compacts clearly indicated the formation of well-crystallized mullite and no other phases were detected. The microstructural features were investigated by scanning electron microscopy, and the findings revealed that the addition of TiO<sub>2</sub> and MoO<sub>3</sub> induced the mullite grains to grow anisotropically. The dielectric characteristics of the sintered samples were measured at increasing frequencies of 100 kHz to 1 MHz. The findings revealed that the mullite sample co-doped with TiO<sub>2</sub> and MoO<sub>3</sub> had the highest dielectric constant of 15.85 and the dielectric loss was 0.93 at 100 kHz.

**Keywords.** Mullite; dielectric properties; characterization.

## 1. Introduction

Mullite is one of the most distinguished materials among the ceramic materials for both traditional and advanced ceramics applications owing to the high melting point (1828 ± 10°C), superior mechanical strength, low thermal expansion coefficient, better creep resistance, high chemical inertness, exceptional resistance to thermal shock and good thermal stability [1–6]. Apart from its use in traditional and refractory-making applications, mullite is extensively used for the manufacture of optical and electronic components, electrical insulators and packaging, ceramic capacitors, protective coatings, radome, solar thermal energy storage units, diesel-particulate filters, components of advanced structural ceramic materials, among others [7–12]. Recent studies have demonstrated that coatings based on mullite ceramics are suitable for various applications [13,14]. The thermal expansion coefficient (TCE) between the substrates and the Si chips needs to be more compatible for supporting the controlled chip connections used in high-package density logic devices. Recent studies have reported that mullite composites have attained the necessary strength and practically match the TCE of silicon chips, compared to alumina [15,16].

Mullite corresponds to the family of aluminosilicates and is generally expressed as Al<sub>4+x</sub>Si<sub>2–2x</sub>O<sub>10–x</sub> (with

0.2 < x < 0.5), which is an oxygen-deficient structure, where x denotes the oxygen vacancy per unit cell. Numerous studies have investigated the effects of adding dopants on the different properties of mullite. A variety of transition metal ions can be accommodated in the mullite structure, by allowing the dopant to form a solid solution with the mullite [17,18]. To date, several studies have ubiquitously investigated the electrical properties of mullite by incorporating transition metal ions into the structure of mullite ceramics synthesized using [19–21] different routes. The incorporation of transition metal ions in the structure of mullite structure has provided persuasive insights into the electrical conductivity at high temperatures and frequencies. The type of transition metal ion and their occupancy in the mullite lattice sites can significantly tailor the physical characteristics of mullite. It has been additionally observed that the reduction in the dielectric constant and loss tangent values of mullite ceramics is within the range necessary for viable applications in electronic industries [22]. Previous studies have demonstrated that the addition of molybdenum salt up to 0.05 molarity and titanium salt up to 0.5 molarity in mullite increases the dielectric constant and loss of tangent values at low frequencies [20,21].

The present investigation aimed to synthesize an extremely pure mullite precursor using the sol–gel method. The study additionally investigated the effects of adding mixed

transition metal ion pairs with higher valence, i.e., co-doping with 1 wt% TiO<sub>2</sub> and 1 wt% MoO<sub>3</sub> on the phase evolution, microstructural property and dielectric behaviour of mullite compact.

## 2. Experimental

### 2.1 Materials

Analytical reagent grade aluminium nitrate nonahydrate (Assay-97.8%; Merck), analytical reagent grade NH<sub>4</sub>Cl (Assay-99.7%; Merck), sodium silicate (Assay of Na<sub>2</sub>O-8% and SiO<sub>2</sub>-26.5%, Loba Chemie), analytical reagent grade ammonium heptamolybdate tetrahydrate (AhM; Merck) and nitric acid (HNO<sub>3</sub>; Merck) were used as the starting materials.

### 2.2 Synthesis of precipitated silica

A 10% aqueous solution of NH<sub>4</sub>Cl was interacted with 50% solution of sodium silicate in a glass jar at pH 6.5 with continuous stirring to prevent gel formation, and subsequently allowed to age for 24 h. The mixture was then filtered through a Whatman-40 filter paper placed over a Buckner funnel under suction, and hot distilled water was used to wash the precipitate. The precipitate was dried for 24 h in an oven at 80°C under vacuum, and subsequently ground and stockpiled in an incubator under a sustained temperature of 35 ± 1°C.

### 2.3 Synthesis of TiO<sub>2</sub> powder

A calculated amount of titanium isopropoxide (TTIP) was dissolved in isopropanol and mixed with distilled water by continual stirring. The pH of the solution was adjusted to 9 by adding NH<sub>4</sub>OH. The solution was then heated to 60–70°C for nearly 24 h. The hydrolysis of TTIP resulted in the precipitation of Ti(OH)<sub>4</sub> and the obtained precipitate was filtered and washed with ethanol. The precipitate was dried in an oven at 80°C under vacuum and synthesized powder was finally calcined at 800°C for 2 h.

### 2.4 Synthesis of MoO<sub>3</sub> powder

For the synthesis of MoO<sub>3</sub> powder, 0.2 M ammonium heptamolybdate tetrahydrate was dissolved in distilled water by mixing with a magnetic stirrer for 30 min. The pH of the solution was carefully adjusted to 3 by adding concentrated HNO<sub>3</sub>. The solution was then heated to a temperature of 60°C for 1 h to form the precipitate. The solution mixture was filtered and repeatedly washed with distilled water and ethanol to remove any unwanted

reactants. The precipitate was dried in an oven under vacuum and subsequently calcined at 800°C for 1 h.

### 2.5 Synthesis of mullite precursor powders

The synthesis of stoichiometric mullite consisted of intensive mixing and dispersion of the required amount of precipitated silica particles into a 0.6 M aqueous solution of AR grade Al(NO<sub>3</sub>)<sub>3</sub> with constant stirring. Diluted ammonia was slowly added to the solution to adjust the pH to 7–8, which was reached and allowed to complete gelation of aluminium hydroxide. The molar ratio of Al<sub>2</sub>O<sub>3</sub>:SiO<sub>2</sub> was carefully adjusted to derive the mullite precursors. The gel mass was allowed to age for 24 h, following which the set gel was filtered through a Whatman-40 filter paper placed over a Buckner funnel under suction. The filter cake was dried for 24 h in an air oven at 70°C under vacuum. The powder was then ground and kept in an incubator.

### 2.6 Preparation of Ti<sup>4+</sup> and Mo<sup>6+</sup> doped mullite precursor powders

For the synthesis of Ti<sup>4+</sup> and Mo<sup>6+</sup> doped mullite precursor powders, the calculated amounts of the synthesized fine powders of MoO<sub>3</sub> and TiO<sub>2</sub> were mixed with the mullite (calcined and uncalcined) precursor powders, followed by milling with a tungsten carbide vial set and media (8000 M, SPEX SamplePrep®, Metuchen, NJ, USA) for 30 min. The synthesized mullite precursors (80%) were precalcined to remove the gel water, and the rest (20%) was intimately mixed with the calcined sample. The process of batch preparation involved close mixing of required quantities of TiO<sub>2</sub>, MoO<sub>3</sub> and mullite (calcined and uncalcined) precursor powders. Batch compositions of undoped and doped mullite are provided in table 1.

Discs of each batch composition were fabricated by applying a uniaxial pressure of 700 kg cm<sup>-2</sup>. Discs of 12 mm diameter were fabricated for each of the batches prepared herein. All the compacts were kept in an air oven at 110°C for 24 h and subsequently fired in an electrically operated programmable muffle furnace at a temperature of 1550°C with a fixed dwelling time of 2 h. The fired discs were removed from the furnace after cooling, and all the characteristics of the fired compacts were determined.

### 2.7 Characterization

The synthesized precipitated silica, MoO<sub>3</sub> and TiO<sub>2</sub> were characterized using surface area analyzer and by X-ray diffraction (XRD) analyses.

The dried mullite precursor powder was examined using a surface area analyzer and particle size analyzer by Fourier-transform infrared (FTIR) spectroscopy and

**Table 1.** Batch compositions (wt%) of undoped and doped mullite.

Batch identity	Calcined mullite	Uncalcined mullite	Titanium dioxide (TiO <sub>2</sub> )	Molybdenum dioxide (MoO <sub>3</sub> )
B-1	80	20	0.00	0.00
B-2	80	20	1.00	1.00

scanning electron microscopy (SEM), respectively. A Malvern Master Sizer, Model X Ver. 1.2b, Serial No. 6449, USA was used to measure the particle size distribution in the range of 0.06 to 6.0  $\mu\text{m}$ . The specific surface area was measured using a Micromeritics Gemini VII surface area analyzer (model number: 2390a). The FTIR spectra were obtained using a PerkinElmer-783 spectrophotometer to identify the nature of the bonds in the mullite precursor powder. The phases of the undoped and doped mullite sintered at 1550°C were identified by XRD analysis using an X-ray diffractometer (Philips X'Pert PRO PW-3071). Scanning electron microscope (ZEISS, INCA Penta FETx3, MODEL, EDS8100, UK) was used to characterize the microstructure of the etched surfaces of each sample, by sintering the sample compacts at 1500°C.

A Wayne Kerr Precision Magnetics Analyzer (3260B) was used to determine the dielectric properties of the co-doped sintered mullite compacts in each batch at a frequency range of 100 Hz to 1 MHz.

### 3. Results and discussion

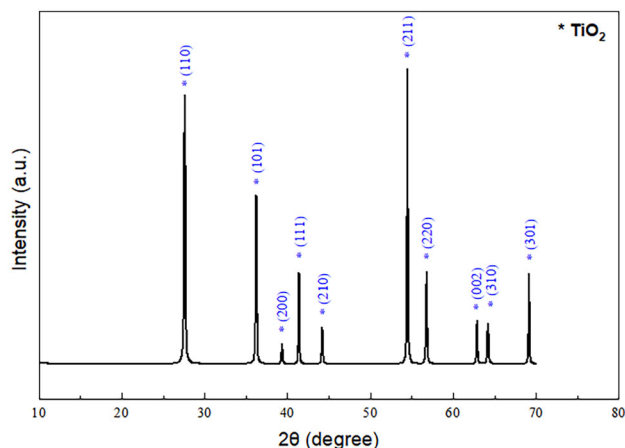
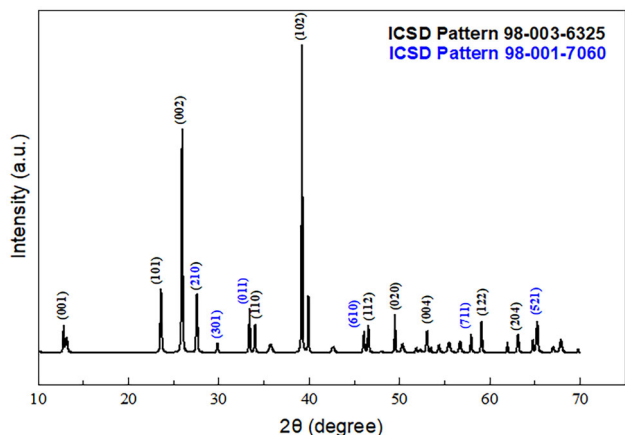
#### 3.1 Evaluation of synthesized powders of precipitated silica, molybdenum oxide and titanium oxide

The synthesized TiO<sub>2</sub> and precipitated silica powders were very soft, lightweight and white in colour, whereas the MoO<sub>3</sub> powder was soft and yellowish-green in colour. The precipitated silica powder essentially consisted of micro-fine silica particles with trace impurities and had a high surface area of 55 m<sup>2</sup> g<sup>-1</sup>, whereas the TiO<sub>2</sub> and MoO<sub>3</sub> powder had specific surface areas of 15.95 and 21 m<sup>2</sup> g<sup>-1</sup>, respectively.

The XRD patterns of the synthesized TiO<sub>2</sub> powder are depicted in figure 1. The observed diffraction pattern at  $2\theta$  angles 27.6°, 36.2° and 54.4° corresponded to the rutile phase, which agrees with the standard reference spectrum (ICCD#01-087-0710).

Comparison of the XRD patterns of the prepared MoO<sub>3</sub> powder (figure 2) with the standard reference pattern revealed the presence of monoclinic (ICCD#98-003-6325) and orthorhombic crystal forms (ICCD#98-001-7060).

The XRD pattern of the synthesized precipitated SiO<sub>2</sub> powder is depicted in figure 3. The shallow pattern with the equivalent Bragg's angle of  $2\theta = 24.051^\circ$  indicated that the material was nearly amorphous. The smoothness of the band also demonstrated that washing multiple times with

**Figure 1.** X-ray diffraction patterns of synthesized TiO<sub>2</sub> powder.**Figure 2.** X-ray diffraction patterns of synthesized MoO<sub>3</sub> powder.

deionized water was effective in removing the NaCl impurities entrapped in the pores of the gel network.

#### 3.2 Characterization of synthesized mullite precursor powder

Mullite was synthesized using a wet interaction technique with pure-grade chemicals, which resulted in very low levels of contamination with impurities. It is assumed that a coating of aluminium hydroxide forms over the fine precipitated silica during the precipitation of aluminium hydroxide by ammonium hydroxide during the wet chemical interaction with the dispersed precipitate. The formed

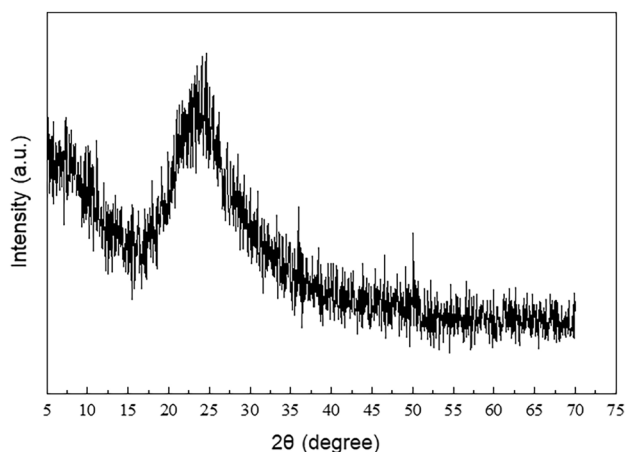


**Figure 3.** X-ray diffraction pattern of synthesized precipitated silica powder.

gel was kept aside for ageing, and subsequently subjected to slow drying to curtail agglomeration. The dried precursor powder was white in colour, had a soft fluffy appearance, and contained fine particles.

**3.2a Particle size distribution and specific surface area:** The particle size distribution (PSD) of the synthesized mullite precursor is depicted in figure 4, and the findings indicated that 50% of the total volume of the particles in the PSD was below 35.5  $\mu\text{m}$ . The precursor powder contained microfine particles with specific surface area (SSA) of 137.70  $\text{m}^2 \text{g}^{-1}$ .

**3.2b Analysis of FTIR spectra:** The distinct IR active bonds in the synthesized mullite precursor were further analysed by FTIR spectroscopy of the samples. The FTIR spectrum of the synthesized mullite precursor is shown in figure 5.

The broad and wide absorption bands in and around 3000 to 3600  $\text{cm}^{-1}$  with wavenumbers of approximately 3456 and

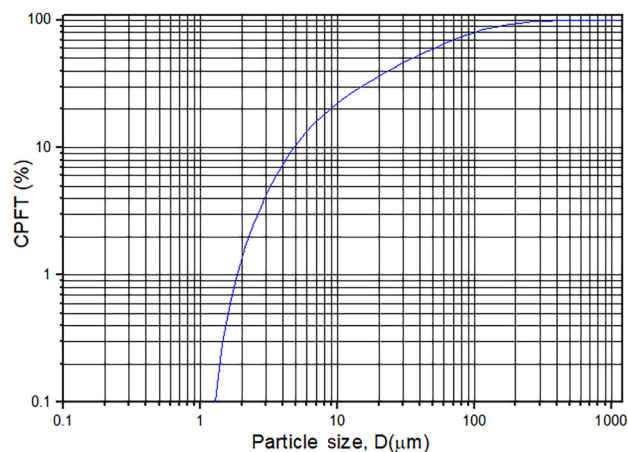


**Figure 4.** Particle size distribution of synthesized mullite precursor.

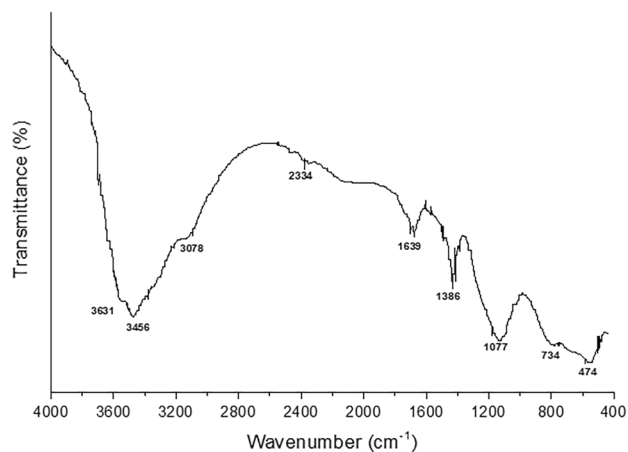


**Figure 5.** FTIR spectrum of synthesized mullite precursor particles.

3357, respectively, corresponded to the stretching bands of the OH groups and water molecules, respectively. The absorption bands at 1638 and 1385  $\text{cm}^{-1}$  corresponded to the bending vibration of water molecules and nitrate groups, respectively. The presence of absorption bands around 2334  $\text{cm}^{-1}$  was attributed to the Si-OH stretching mode, whereas those at 1077  $\text{cm}^{-1}$  corresponded to the bending modes of Si-OH. The stretching bands at 734 and 474  $\text{cm}^{-1}$  corresponded to the Al-O-Al and Si-O-Si linkages, respectively, in the gel network.

### 3.3 XRD analysis

The different phases of the mullite powder and the effects of the co-dopants on the crystallization of mullite powder were identified by XRD analyses. The X-ray diffractograms are depicted in figure 6, and the results demonstrated that mullite was the main phase. The XRD spectra of the compacts sintered at 1550°C contained prominent peaks at

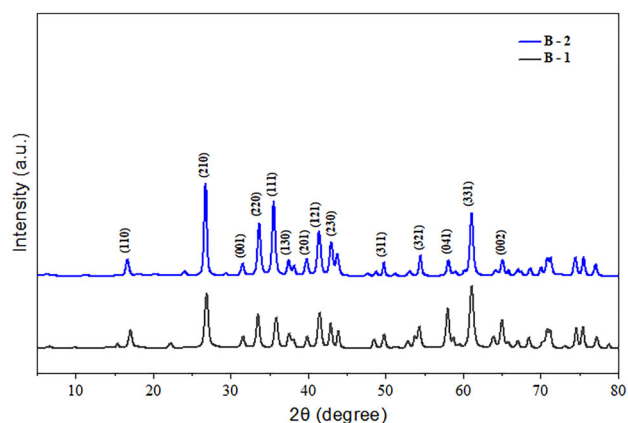


**Figure 6.** X-ray diffraction patterns of undoped mullite compact sample (B-1) and co-doped mullite compact sample (B-2) heat treated at 1550°C.

$2\theta \sim 26.7^\circ, 33.6^\circ, 35.5^\circ$  and  $41.2^\circ$ , which corresponded to the (210), (220), (111) and (121) planes of mullite (JCPDS #15-0776), respectively. The co-doped metal ions had a ‘mineralizing’ effect, which positively influenced the phase transformation of mullite and has been previously reported by several studies [16,19–21]. The structural rearrangement caused by the incorporation of transition metal ions that interacted with the alumina and silica in the precursor powders accelerated the transformation of the mullite phase [23–26].

No secondary phases associated with  $\text{MoO}_3$  and  $\text{TiO}_2$  were observed in the XRD spectra, and this could be attributed to the very low concentration of dopants used in this study. This co-doped mullite may be defined as a solid solution of transition metal ions within the mullite lattice.

The crystallite sizes of the undoped mullite and mullite co-doped with transition metal ions were determined by using the Scherrer formula (equation 1).

$$d = \frac{0.89\lambda_{\text{Cu}}K_\alpha}{B_\beta \cos \theta_B} \quad (1)$$

where  $d$  represents the crystallite size,  $\lambda_{\text{Cu}}K_\alpha$  is the wavelength of the X-ray with Cu target,  $B_\beta$  represents the full-width at half-maximum of the most intense peak (in rad), and  $\theta_B$  is half of the corresponding diffraction angle (in rad). The average crystallite size decreased from 115.21 to 190.19 nm following the addition of dopants, which indicated that an increase in the concentration of co-dopants improved the crystallinity at  $1550^\circ\text{C}$ .

### 3.4 Dielectric study

The dielectric constant is one of the most vital properties of ceramic materials and typically defines how energy is stored and transferred within substances. Figure 7 provides the dielectric constants of an undoped mullite sample and a

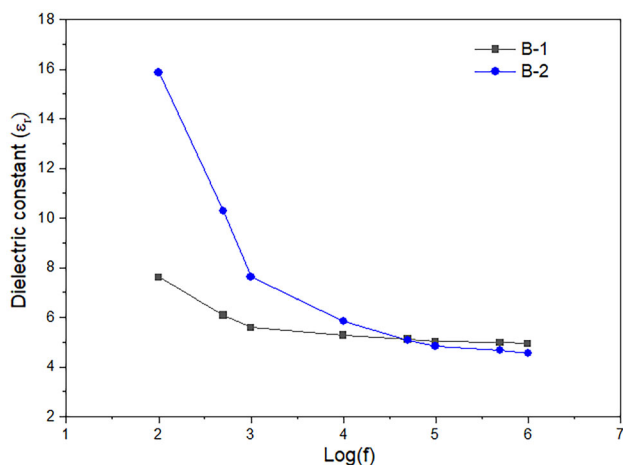


**Figure 7.** Variation of dielectric constant with frequency of undoped mullite compact sample (B-1) and co-doped mullite compact sample (B-2) heat treated at  $1550^\circ\text{C}$ .

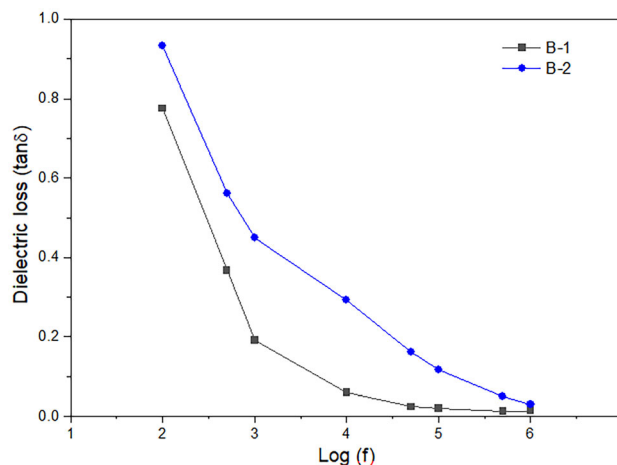


**Figure 8.** Variation of dielectric loss with frequency of undoped mullite compact sample (B-1) and co-doped mullite compact sample (B-2) heat treated at  $1550^\circ\text{C}$ .

co-doped sintered mullite compact as a function of increasing frequency. It was evident from the plot that the dielectric constant was indirectly proportional to the frequency in both batches.

The electron-hopping model elucidates the process of polarization due to electrical conduction in mullite co-doped with titanium and molybdenum [27]. This behaviour was probably attributed to the fact that the oxygen atoms in mullite systems tend to move towards the oxygen vacancies through the tetrahedral double chains in the structure of mullite. In batch B-2, the lower valent  $\text{Al}^{3+}$  was substituted by higher valent transition metal ions ( $\text{Ti}^{4+}$  and  $\text{Mo}^{6+}$ ), which created more oxygen vacancy of the mullite system. Therefore, the co-doping of metal ions within the mullite system led to oxygen hopping, which further increased the dielectric constant compared to the batch of undoped mullite (B-1). This effect was caused by polarization and reduced the field within the medium [22,28]. The findings revealed that the doped sample (B-2) had a dielectric constant of 15.85, which was attributed to the higher polarization of the  $\text{Ti}^{4+}$  and  $\text{Mo}^{6+}$  metal ions within the material, as metal oxides generally have a high dielectric constant. Due to electronic polarizations, the dielectric constant of a material can decrease significantly at increased frequencies before attaining a constant value. Individual dipoles can align themselves with the electric field at lower frequencies due to electronic polarizations but are unable to move instantaneously at higher frequencies. This leads to a decline in the dielectric constant at increasing frequencies [29]. The frequency-dependent changes in dielectric behaviour are further explained by the Maxwell-Wagner model [30]. The theory holds that the dielectric system consists of different grains where poorly conducting grain boundaries separate the high-conducting grains. The charges may readily move across the conducting grains when the system

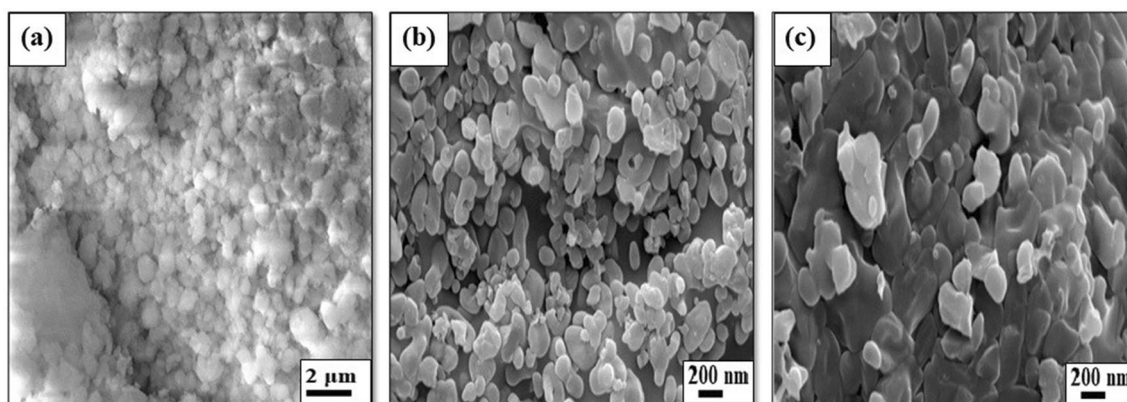


**Figure 9.** SEM micrographs of (a) mullite precursor dried at 110°C, (b) undoped mullite compact sample heat treated at 1550°C, and (c) co-doped mullite compact sample heat treated at 1550°C.

is subjected to an external electric field but can build up on the grain boundaries, causing significant polarization and increasing the dielectric constant [31].

The loss factor of a substance is defined as the energy loss in terms of heat from the material. The dielectric loss ( $\tan\delta$ ) with the loss tangent values depends on the stability between the increasing amount of mullite, the effect of lower porosity and the higher content of the glassy phase, which is proportional to the imaginary part of the dielectric constant.

The dielectric losses of both batches were measured between frequencies of 100 Hz and 1 MHz at room temperature. The dielectric losses ( $\tan\delta$ ) of all the samples plotted against increasing frequencies are depicted in figure 8.

The results demonstrated that  $\tan\delta$  decreased at increasing frequencies and was lowest at a frequency of 1 MHz. The movement of the mobile ions, namely,  $\text{Al}^{3+}$  in the undoped batch (B-1), and  $\text{Al}^{3+}$ ,  $\text{Mo}^{6+}$  and  $\text{Ti}^{4+}$  in the co-doped batch (B-2), and the losses resulting from the deformation of the silica network structure were typically responsible for the dielectric loss of the mullite system. This mechanism, which involves electrical conduction, can be responsible for such behaviour of mullite.

The increase in polarization was attributed to the alignment of dipoles with the electric field and could be responsible for the increase in dielectric loss at low frequencies. An increase in the frequency limits the dipole response as the electrical dipole aligns with the electric field and explains why the dissipation factor decreases at increasing frequencies [32–34].

This aspect of loss tangent is supported by Koop's theory, which explains that when grain boundary resistivity is relatively high at lower frequencies, energy losses are significant compared to high frequencies as resistivity is less [35].

### 3.5 Microstructural characterization

The morphology of all the batches of synthesized mullite and sintered mullite compact co-doped with metal ions was

investigated by SEM, as depicted in figure 9. The findings revealed that the powder particles were spherical in appearance, and several smaller agglomerations were observed.

Microstructural images revealed the presence of lathe-like, unevenly distributed mullite grains in undoped mullite (figure 9b). However, the size of the mullite grains increased anisotropically following the addition of both  $\text{TiO}_2$  and  $\text{MoO}_3$ , but the porosity reduced with a gradual increase in density, which indicated that the mixture of metal ions catalysed the grain growth. Co-doping with 1.00 wt%  $\text{TiO}_2$  and 1.00 wt%  $\text{MoO}_3$  increased the aspect ratio of the mullite grain, induced grains elongated with better packing, and drastically reduced the pores (figure 9c). These changes could be attributed to the effect of  $\text{TiO}_2$ , which catalysed the grain growth in the mullite system.

## 4. Conclusion

In this study, a mullite ceramic powder derived using the sol–gel method was co-doped with synthetically prepared powders of the transition metal oxides, i.e., titanium ( $\text{Ti}^{4+}$ ) and molybdenum ( $\text{Mo}^{6+}$ ), and fabricated into compacts. The compacts were subjected to sintering at 1550°C to investigate their phase evolution, microstructure and dielectric properties. XRD spectroscopy revealed that crystallized mullite was the only phase detected in the sintered co-doped mullite ceramic. It is possible that a solid solution of metal ions formed within the mullite system, which accounted for the absence of other phases. An increase in metal ion content indicated that the process of mullitization was accelerated, which was subsequently confirmed by the XRD spectroscopy and analyses of the microstructural characteristics by SEM images. Analysis of the SEM micrographs further revealed that the inclusion of a relatively small amount of titania accelerated the growth of mullite grains. This transition metal ion-dependent electrical behaviour was observed for co-doped mullite

ceramic from the experimental plots. The dielectric constants and dielectric losses of the doped and undoped mullite decreased with increasing of frequencies and became constant at a high frequency. The dielectric constants of mullite ceramics co-doped with titanium ( $Ti^{4+}$ ) and molybdenum ( $Mo^{6+}$ ) were higher than that of the undoped mullite owing to the greater extent of polarization of these metal ions within the material.

## References

- [1] Aksaf A and Pask J A 1975 *J. Am. Ceram. Soc.* **58** 507
- [2] Kanka B and Schneider H 1994 *J. Mater. Sci.* **29** 1239
- [3] Song K C 1998 *Mater. Lett.* **35** 290
- [4] Aksay L A, Dabbs D M and Sarikaya 1991 *J. Am. Ceram. Soc.* **74** 2343
- [5] Imose M, Takano Y, Yoshinaka M, Hirota K and Yamaguchi O 1998 *J. Am. Ceram. Soc.* **81** 1537
- [6] Sanyal D, Banerjee D, Bhattacharya R, Patra S K, Chaudhuri S P, Nandi Ganguly B *et al* 1996 *J. Mater. Sci.* **31** 3447
- [7] Biswal B and Mishra D K 2022 *Ceram. Int.* **48** 9765
- [8] Omerašević M, Kocjan A and Bučevac D 2022 *Ceram. Int.* **48** 2273
- [9] Roy R, Das D and Rout P K 2022 *Eng. Sci.* **18** 20
- [10] Viswabaskaran V, Gnanam F D and Balasubramanian M 2004 *Appl. Clay Sci.* **25** 29
- [11] Ecebaş N, Dursun G M, Yeşilova A H and Duran C 2020 *Int. J. Appl. Ceram. Technol.* **17** 264
- [12] Xu X, Zhang Y, Wu J, Hu C and Tang Z 2017 *Int. J. Appl. Ceram. Technol.* **14** 162
- [13] Chen X, Zheng W, Zhang J, Liu C, Han J, Zhang L *et al* 2020 *Ceram. Int.* **46** 11819
- [14] Lee K N 2000 *J. Eng. Gas Turbines Power* **122** 632
- [15] Kurihara T, Horiuchi M, Takeuchi Y and Wakabayashi S 1990 *40th IEEE Conference Proceedings on Electronic Components and Technology* p 68
- [16] Camerucci M A, Urretavizcaya G, Castro M S and Cavalieri A L 2001 *J. Eur. Ceram. Soc.* **21** 2917
- [17] Schneider H and Komarneni S 2006 *Mullite*. Wiley, Weinheim
- [18] Sarin P, Yoon W, Haggerty R P, Chiritescu C, Bhorkar N C and Kriven W M 2008 *J. Euro. Ceram. Soc.* **28** 353
- [19] Chaudhuri S P and Patra S K 1997 *Br. Ceram. Trans.* **96** 105
- [20] Paul B K, Haldar K, Roy D, Bagchi B, Bhattacharya A and Das S 2014 *J. Adv. Ceram.* **3** 278
- [21] Halder K, Roy D and Das S 2015 *J. Mater. Sci. Mater. Electron* **26** 5803
- [22] Silva V J, Almeida E P, Gonçalves W P, Nóbrega R B, Araújo N G, Lucena L H *et al* 2019 *Ceram. Int.* **45** 4692
- [23] Da Silva M G F 1998 *J. Sol-Gel. Sci. Technol.* **13** 987
- [24] Schneider H, Fischer R X and Schreuer J 2015 *J. Am. Ceram. Soc.* **98** 2948
- [25] Esharghawi A, Penot C and Nardou F 2009 *J. Eur. Ceram. Soc.* **29** 31
- [26] Bagchi B, Das S, Bhattacharya A, Basu R and Nandy P 2009 *J. Am. Ceram. Soc.* **92** 748
- [27] Jonker G H and Houten S V 2008 In: *Advances in solid state physics* F Sauter (ed) (Berlin: Springer) p 118
- [28] Sindhu S, Anantharaman M R, Thampi B P, Malini K A and Kurian P 2002 *Bull. Mater. Sci.* **25** 599
- [29] Abdel-Hameed S A M, Morsi R M M and Margha F H 2017 *J. Mater. Sci. Mater. Electron* **28** 4351
- [30] Wagner K W 1973 *Annals Phys.* **40** 817
- [31] Mansour S F 2005 *Egypt. J. Solids* **28** 263
- [32] Heikes R R and Johnston W D 1957 *J. Chem. Phys.* **26** 582
- [33] Venkataraju C, Sathishkumar G and Sivakumar K 2010 *J. Alloys Compd.* **498** 203
- [34] Punithavathy I K, Rajeshwari A, Jeyakumar S J, Lenin N, Vigneshwaran B, Jothibas M *et al* 2020 *J. Mater. Sci. Mater. Electron* **31** 9783
- [35] Koops C G 1951 *Phys. Rev.* **83** 121

Springer Nature or its licensor (e.g. a society or other partner) holds exclusive rights to this article under a publishing agreement with the author(s) or other rightsholder(s); author self-archiving of the accepted manuscript version of this article is solely governed by the terms of such publishing agreement and applicable law.